



# Investigation of the Application and Mechanism of Nitrogen and Phosphorus Co-doped Carbon Dots for Mercury Ion Detection

Dong Yang<sup>1,2</sup> · Chaoqun Ma<sup>1,2</sup> · Guoqing Chen<sup>1,2</sup> · Lei Li<sup>1,2</sup> · Anqi Hu<sup>1,2</sup> · Anlan Huang<sup>1,2</sup> · Yan zhou<sup>1,2</sup> · Zicheng Cai<sup>1,2</sup> · Taiqun Yang<sup>1,2</sup> · Hui Gao<sup>1,2</sup> · Jiao Gu<sup>1,2</sup> · Chun Zhu<sup>1,2</sup> · Yamin Wu<sup>1,2</sup>

Received: 13 December 2023 / Accepted: 17 January 2024

© The Author(s), under exclusive licence to Springer Science+Business Media, LLC, part of Springer Nature 2024

## Abstract

In this paper, we obtained nitrogen and phosphorus co-doped carbon dots through a hydrothermal method using o-phenylenediamine and citric acid in a 40% phosphoric acid environment. The carbon dots emitted fluorescence at 476 nm under excitation at 408 nm and exhibited good selectivity and high sensitivity towards mercury ions. These carbon dots showed excellent dispersibility in water and maintained stable fluorescence even in high concentration salt environments. The interaction between mercury ions and functional groups on the carbon dots surface through electrostatic interaction resulted in static quenching. Simultaneously, by detecting the lifetime and transient absorption spectra of the carbon dots, we observed that the coordination of mercury ions with the carbon dots broadened the band structure of the carbon dots, and the existing photoinduced electron transfer process increased the non-radiative transition channel. The combined effect of dynamic quenching and static quenching significantly reduced the fluorescence intensity of the carbon dots at 476 nm. The carbon dots exhibited linear detection of mercury ions in the range of 0.01–1  $\mu\text{M}$ , with a detection limit as low as 0.0245  $\mu\text{M}$ . In terms of practical water environmental detection applications, these carbon dots were able to effectively detect mercury ions in tap water and lake water, demonstrating their broad application prospects in the field of environmental metal analysis.

**Keywords** Fluorescence probe · Mercury ion detection · Dynamic quenching · Static quenching · Transient absorption

## Introduction

The excessive emission of heavy metal ions caused by large-scale industrialization has had a severe impact on human health and environmental safety [1, 2]. Therefore, trace detection of heavy metal ions is of great significance, particularly in fields such as medicine, biology, and environmental science. Mercury (Hg) is one of the main pollutants in the environment and one of the most common and dangerous metal ions. In the ecological environment, mercury can

maintain long-term relative stability [3]. Additionally, different oxidation states of mercury are toxic and can accumulate in organisms, causing damage to the organs of animals and humans [4]. Therefore, it is crucial to study economical, convenient, and sensitive methods for detecting  $\text{Hg}^{2+}$ . Researchers have proposed various methods to determine different forms of  $\text{Hg}^{2+}$ , including atomic absorption spectroscopy (AAS), X-ray fluorescence spectroscopy (XRF), and atomic fluorescence spectroscopy (AFS) [2]. In addition, detection methods for  $\text{Hg}^{2+}$  based on surface-enhanced Raman spectroscopy (SERS), colorimetry, electrochemical techniques, and surface plasmon resonance sensors have also been developed [2, 5, 6]. These techniques differ in sensitivity, selectivity, accuracy, and detection time, and they have certain problems, such as low reproducibility and complex technical processes [6]. In contrast, many metal ion sensors are designed using fluorescence probe technology because this method is simple and has good sensitivity, selectivity, reproducibility, as well as significant advantages in terms of detection speed, non-destructive testing, and economics

✉ Chaoqun Ma  
machaoqun@jiangnan.edu.cn

Lei Li  
lli@jiangnan.edu.cn

<sup>1</sup> School of Science, Jiangnan University, Wuxi 214122, China

<sup>2</sup> Jiangsu Provincial Research Center of Light Industrial Optoelectronic Engineering and Technology, Wuxi 214122, China

[7–11]. In this study, we synthesized a simple and low-cost carbon dots (CDs) probe using a bottom-up strategy. In a phosphoric acid solution environment, we synthesized CDs with high selectivity and sensitivity towards  $\text{Hg}^{2+}$  using solvent-thermal method, *o*-phenylenediamine, and citric acid. The CDs solution emitted blue fluorescence under excitation at 407 nm and exhibited an “on-off” response towards  $\text{Hg}^{2+}$ . We observed a good linear relationship in the range of 10–1000 nM and calculated a detection limit of 24.5 nM. The application of these CDs in the detection of  $\text{Hg}^{2+}$  in practical water environments showed tremendous potential for the new fluorescent probe in terms of reliability, visual detection, and selective detection.

## Materials and Methods

### Reagents

All reagents used in the experiments were of analytical grade and were provided by Sinopharm Chemical Reagent Co., Ltd. The reagents used were *o*-phenylenediamine, citric acid, phosphoric acid,  $\text{Hg}(\text{NO}_3)_2 \cdot \text{H}_2\text{O}$ ,  $\text{AlCl}_3$ ,  $\text{CaCl}_2$ ,  $\text{Cd}(\text{NO}_3)_2 \cdot 4\text{H}_2\text{O}$ ,  $\text{CoCl}_2$ ,  $\text{CuCl}_2 \cdot 2\text{H}_2\text{O}$ ,  $\text{FeCl}_2 \cdot 4\text{H}_2\text{O}$ ,  $\text{FeCl}_3 \cdot 6\text{H}_2\text{O}$ ,  $\text{MgCl}_2$ ,  $\text{Pb}(\text{NO}_3)_2$ ,  $\text{ZnCl}_2$ ,  $\text{NaCl}$ ,  $\text{NaOH}$ , and  $\text{HCl}$ . Ultrapure water (18.2 M $\Omega$ /cm) was used as the experimental water.

### Apparatus

We used a JEM-2100 F transmission electron microscope (JEOL, Japan) to capture high-resolution transmission electron microscope images of CDs. To obtain information about the elemental composition and functional groups of the CDs, we used the ESCALAB 250Xi photoelectron spectrometer (Thermo Fisher Scientific, USA) to record X-ray photoelectron spectroscopy (XPS) and the Frontier infrared spectrometer (Perkin-Elmer, USA) to obtain the Fourier transform infrared spectroscopy (FTIR) of CDs. The fluorescence spectrum and ultraviolet-visible (UV-Vis) absorption spectrum of the samples were measured using

the FS5 fluorescence spectrometer (Edinburgh Instruments, UK) and UV-2600 UV-Vis spectrophotometer (Shimadzu, Japan), respectively. The fluorescence lifetime information of the samples was obtained using the FLS920 steady-state/transient fluorescence spectrometer (Edinburgh Instruments, UK). The Zeta potential of the samples was studied using the Zetasizer Nano ZS90 nanoparticle size and zeta potential analyzer (Malvern Instruments Ltd., UK). The femto-second transient absorption spectrometer was developed by the research group, and the light source was sourced from Coherent.

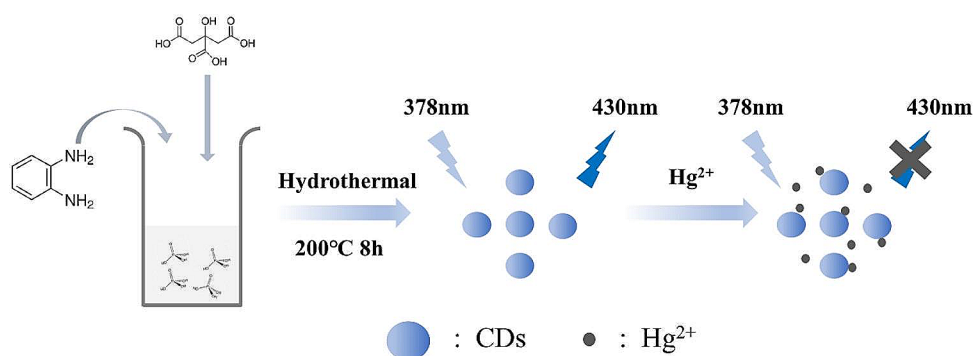
### Synthesis of CDs

We synthesized CDs using a hydrothermal method. 0.108 g of *o*-phenylenediamine and 0.192 g of citric acid were dissolved in 9 milliliters of a 40% concentration phosphoric acid solution (Fig. S1), and the mixture was vigorously shaken for 5 min and then sonicated at room temperature for 15 min to ensure thorough mixing. The mixture was then transferred to a 25-milliliter PTFE-lined autoclave and heated at 200 °C for 8 h to obtain crude CDs (Fig. 1). Silica gel column chromatography with ethyl acetate as the mobile phase was used to remove colored impurities. Finally, the CDs were concentrated using a rotary evaporator. The obtained CDs were stored in a low-temperature refrigerator for subsequent characterization and use.

### Stability and Selectivity of CDs

To investigate the fluorescence stability of CDs under different salt concentrations, we measured the changes in fluorescence intensity within the range of 0 to 1.0 M  $\text{NaCl}$  concentration. To explore the influence of solution pH on the fluorescence intensity of CDs, we prepared buffer solutions with pH ranging from 3 to 12 using 0.1 M  $\text{NaH}_2\text{PO}_4$  and 0.1 M  $\text{Na}_2\text{HPO}_4$  solutions. To validate the selectivity of CDs for  $\text{Hg}^{2+}$ , we selected 10 common interfering cations including  $\text{Al}^{3+}$ ,  $\text{Ca}^{2+}$ ,  $\text{Cd}^{2+}$ ,  $\text{Co}^{2+}$ ,  $\text{Cu}^{2+}$ ,  $\text{Fe}^{2+}$ ,  $\text{Fe}^{3+}$ ,  $\text{Mg}^{2+}$ ,  $\text{Pb}^{2+}$ , and  $\text{Zn}^{2+}$ . Under pH 8 conditions, each metal ion at a

**Fig. 1** The schematic diagram of the synthesis of CDs and its application in  $\text{Hg}^{2+}$  detection



concentration of 1 mM was incubated with the CDs. Subsequently, the fluorescence spectra of the solutions were measured under excitation at 378 nm, and the fluorescence intensities at 430 nm were recorded. In the experiment to measure the detection limit of  $\text{Hg}^{2+}$ , the CDs solution was diluted 800 times and mixed with different concentrations of  $\text{Hg}^{2+}$  solution and a pH 8 buffer solution in a volume ratio of 1:1:8. The above samples were then subjected to fluorescence spectroscopic analysis with an excitation wavelength of 378 nm and an emission wavelength range of 390–550 nm. Each experiment was repeated three times. The calculation formula for the limit of detection (LOD) is  $\text{LOD} = 3\sigma/s$ , where  $\sigma$  represents the standard deviation of three blank samples and  $s$  is the slope of the calibration curve.

### Actual Measurements

To evaluate the feasibility of this method for the detection of  $\text{Hg}^{2+}$  in environmental water samples, we conducted tests on tap water and lake water samples. Tap water samples were obtained from our laboratory, while lake water samples were obtained from the university's lakes. Before analysis, the lake water samples were centrifuged at 11,000 rpm for 10 min and filtered three times using a 0.22  $\mu\text{m}$  microporous membrane. To calculate the recovery rate based on this determination, different concentrations of standard  $\text{Hg}^{2+}$  solutions were added to the environmental water samples for testing. All analysis methods were carried

out as described in the previous section. Each experiment was repeated three times.

## Results and Discussion

### Characterizations of CDs

Characterization through TEM (Fig. 2a) shows that the CDs exhibit a near-spherical appearance and can be uniformly dispersed in the solution. The size distribution ranges from 5 to 6.5 nm, with a relatively concentrated size distribution and an average size of 5.74 nm. HRTEM reveals that the synthesized CDs have a typical lattice structure with a lattice spacing of 0.3 nm corresponding to the plane lattice spacing of graphite (002) [12]. Infrared absorption spectroscopy (Fig. 2c) was used to analyze the composition of the CDs. The results show a broad absorption band in the range of  $2700\text{ cm}^{-1}$ – $3600\text{ cm}^{-1}$  [13], representing the presence of N-H and O-H. An absorption peak is observed at  $1640\text{ cm}^{-1}$ , representing the stretching vibration of  $\text{C}=\text{O}$  or the bending vibration of N-H. Strong absorption is observed at  $1142\text{ cm}^{-1}$  and  $1008\text{ cm}^{-1}$ , corresponding to C-O and N-P, respectively [14, 15].

XPS analysis (Fig. 2d) reveals the presence of various functional groups in the CDs. The binding energies of 134.43 eV, 191.98 eV, 285.17 eV, 401.19 eV, and 532.71 eV correspond to P 2p, P 2s, C 1s, N 1s, and O 1s, respectively.

**Fig. 2** a TEM image of CDs. b Corresponding size distribution of CDs, c FT-IR spectrum of CDs, d XPS spectrum of CDs

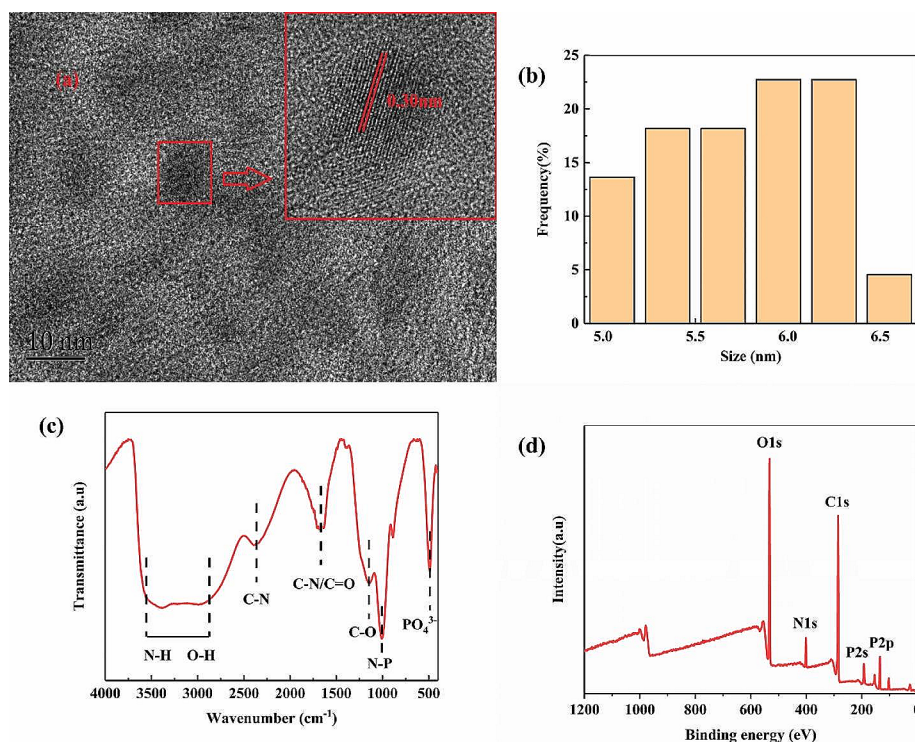


**Fig. 3** **a** Excitation spectrum, emission spectrum and steady-state UV-Vis absorption spectrum of CDs. **b** Steady-state three-dimensional fluorescence spectrum

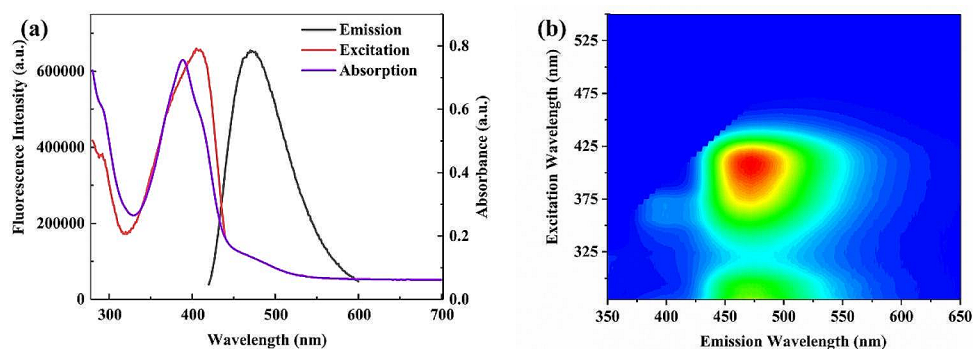
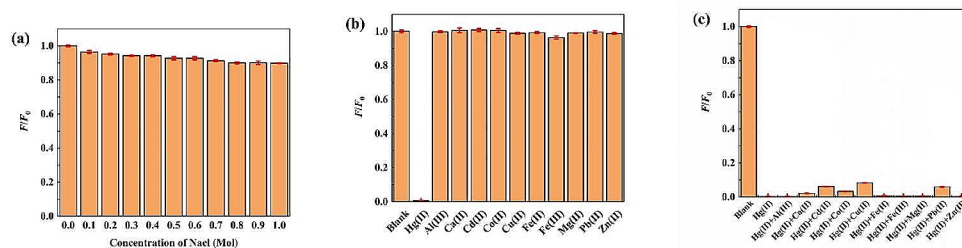


**Fig. 4** **a** Fluorescence intensity ratio of CDs in different concentrations of NaCl solution. **b** The selectivity of CDs for  $\text{Hg}^{2+}$  against other metal ions. **c** Anti-interference ability of CDs



In the C1s region, the fitting peaks at 284.8 eV, 286.02 eV, 287.72 eV, and 289.25 eV correspond to C=C/C-C, C-N/C-O, O-C=O and C=C-N, respectively. The fitting peak at 401.10 eV in the N1s region is mainly attributed to C3-N (graphitic nitrogen). In the O1s region, the fitting peaks at 531.12 eV and 532.60 eV correspond to P=O and O=C-O\*, respectively. The fitting peak at 134.34 eV in the P2p region is attributed to P-O or P-C bonds (Fig. S2) [16, 17].

### Optical Properties of CDs

Numerous research reports have shown that the core and surface states of CDs, as well as their surface functional groups, play important roles in their absorption spectra [18]. As shown in Fig. 3a, the UV-visible absorption spectrum reveals clear absorption peaks of the CDs at 280 and 360 nm–420 nm. The peak centered at 280 nm is attributed to the  $\pi\text{-}\pi^*$  transition of aromatic C=C, while the absorption band in the range of 360–420 nm corresponds to the  $n\text{-}\pi^*$  transition of C=O or the  $\text{sp}^3$  hybridization of C–OH on the CDs' surface [19]. The steady-state fluorescence excitation spectrum and steady-state absorption spectrum exhibit significant overlap in the range of 350–410 nm, indicating that the fluorescence of the CDs is mainly caused by surface defects [20]. A strong excitation peak is observed at 408 nm, and the emission peak is located at 472 nm. The three-dimensional fluorescence spectrum displayed in the right panel shows that the emission wavelength of the CDs remains stable at different excitation wavelengths.

### Fluorescence Detection of $\text{Hg}^{2+}$

stability and ion interference experiments of the CDs were conducted. As shown in Fig. 4a, the fluorescence intensity of the CDs remains relatively unchanged with increasing NaCl concentration, indicating good salt resistance. Among various metal ions added to the solution of CDs, only  $\text{Hg}^{2+}$  exhibits a significant quenching effect, while other ions have little interference with the fluorescence of CDs, indicating good selectivity. When both other ions and  $\text{Hg}^{2+}$  are simultaneously added to the solution of CDs, the fluorescence quenching effect is significant, further demonstrating the good anti-interference performance of the CDs.

pH optimization experiments were conducted on the CDs (Fig. 5). The emission peak of CDs is significantly enhanced and accompanied by a blue shift as the pH of the CDs solution changes from 3 to 12. When pH = 8, the quenching rate of CDs reaches its maximum, and the fluorescence intensity is higher. Under acidic conditions (pH < 7), the fluorescence intensity of CDs slightly decreases and shows a red shift phenomenon, which may be caused by the binding of -COOH on the surface of CDs and  $\text{H}^+$ , leading to excited proton transfer [21]. The PL of CDs under alkaline conditions mainly depends on  $\beta$ -dicarbonyl groups, while carboxyl and hydroxyl groups contribute relatively less [21]. The fluorescence intensity has no significant alteration with the increase of pH from 7 to 12, indicating that the amount of  $\beta$ -dicarbonyl on the surface of CDs is small [18, 22]. Therefore, pH = 8 was used in subsequent experiments.



**Fig. 5** **a** Emission spectra of CDs in different pH environments. **b** Quenching degree of CDs with the addition of  $\text{Hg}^{2+}$  in different pH environments

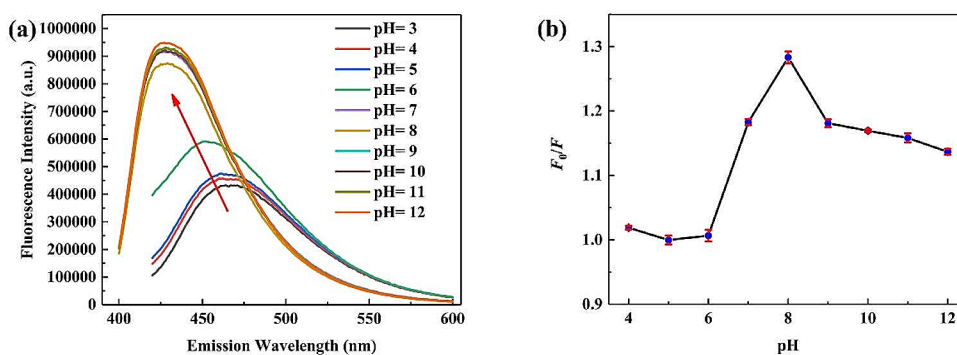


**Fig. 6** **a** Emission spectra of CDs after the addition of 0-1000 nM  $\text{Hg}^{2+}$ . **b** The relationship between the fluorescence quenching degree and the concentration of  $\text{Hg}^{2+}$  (Inset: the linear relationship between the fluorescence quenching degree and the concentration of  $\text{Hg}^{2+}$  in the range of 10-1000 nM)

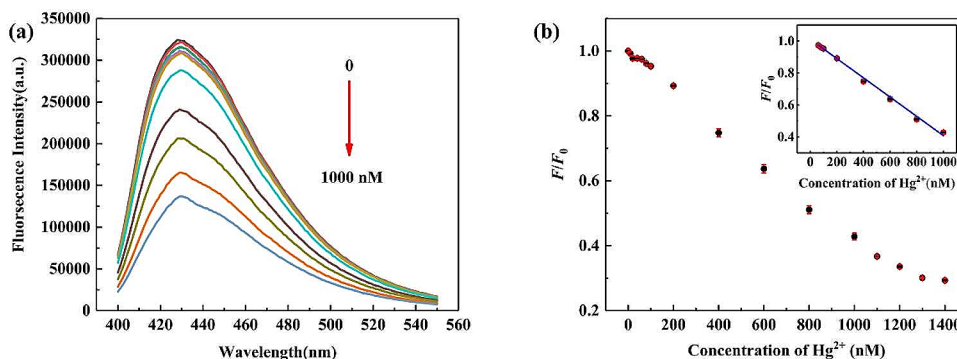


**Fig. 7** **a** Steady-state absorption spectra of CDs with and without the addition of  $\text{Hg}^{2+}$ . **b** Fluorescence lifetime test of CDs with and without the addition of  $\text{Hg}^{2+}$

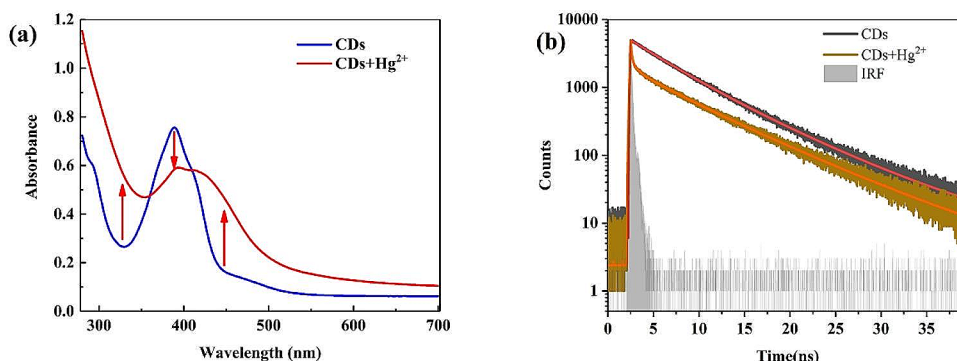


**Table 1** Analysis of fluorescence lifetime components of CDs before and after adding  $\text{Hg}^{2+}$

	Comp.1	Comp.2	
$\alpha(\%)$	36.62	63.38	
Alpha	0.009616	0.016641	
Tau(ns)	7.81	4.29	
	Comp.1	Comp.2	Comp.3
$\alpha(\%)$	45.25	29.41	25.34
Alpha	0.003535	0.002298	0.00198
Tau(ns)	7.81	4.29	0.58

Additionally, we further studied the relationship between  $\text{Hg}^{2+}$  concentration and CDs fluorescence quenching degree (Fig. 6). The experimental results show that the fluorescence intensity of CDs gradually weakens as the  $\text{Hg}^{2+}$  concentration increases from 0 to 1000 nM. Moreover, within the range of 10-1000 nM, the quenching degree of CDs exhibits

a good linear relationship with  $\text{Hg}^{2+}$  concentration. Through linear fitting, we calculated the detection limit of  $\text{Hg}^{2+}$  to be 24.5 nM.

### Possible Mechanism of $\text{Hg}^{2+}$ Sensing

We subsequently revealed the mechanism of  $\text{Hg}^{2+}$  quenching CDs fluorescence through various means. Zeta potential analysis (Fig. S3) showed that the CDs solution was negatively charged. After the addition of  $\text{Hg}^{2+}$ , the solution remained negatively charged, but the absolute value decreased, indicating that the stability of the solution decreased and complexation occurred between the CDs and  $\text{Hg}^{2+}$ . The steady-state absorption results are shown in Fig. 7a. After the addition of  $\text{Hg}^{2+}$ , the peak intensity of

**Fig. 8** Three-dimensional transient absorption spectra of CDs before and after addition of  $\text{Hg}^{2+}$  **a** before **c** after. Transient absorption spectra of typical moments of CDs before and after addition of  $\text{Hg}^{2+}$  **b** before **d** after

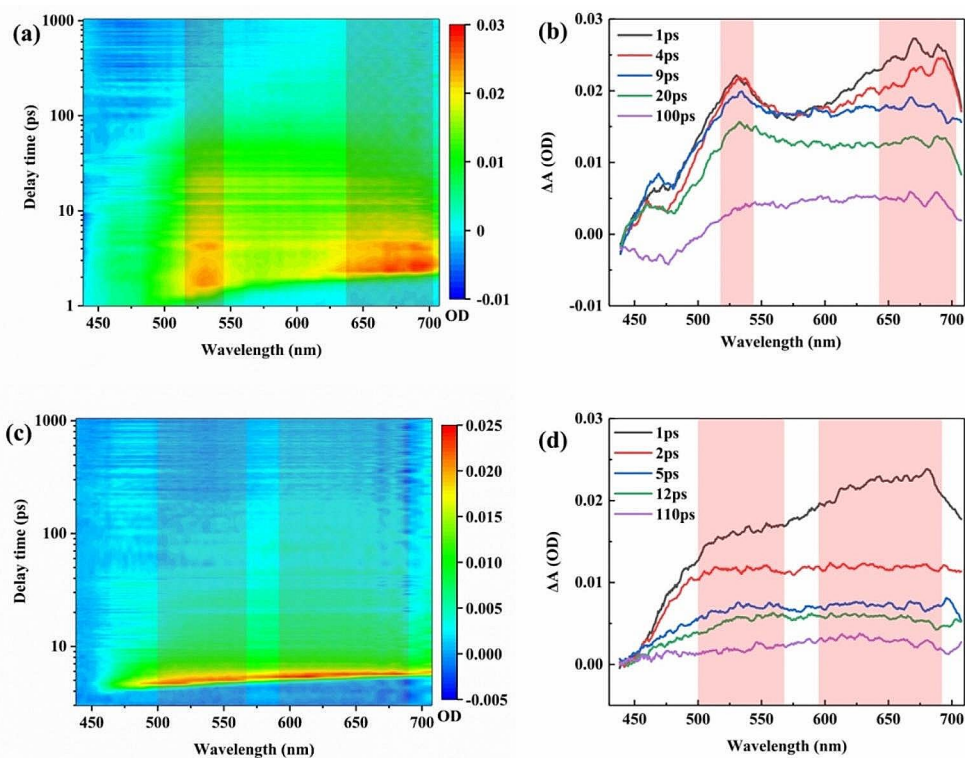


**Table 2** Global fitting component analysis of transient absorption spectra before and after the addition of  $\text{Hg}^{2+}$

	Comp.1	Comp.2	Comp.3
Alpha	0.000154949	0.0142942	0.170527
Tau(ps)	6453.72	69.96	5.86
	Comp.1	Comp.2	Comp.3
Alpha	0.00191473	0.0754079	0.924438
Tau(ps)	522.27	13.26	1.08

the broad absorption peak at 380 nm in the CDs solution decreased, the absorption band widened, and the absorption in the short-wavelength region below 320 nm strengthened. This further indicates the formation of a complex between the CDs and  $\text{Hg}^{2+}$ , resulting in static quenching. The fluorescence lifetime analysis results are shown in Fig. 7b. After the addition of  $\text{Hg}^{2+}$ , the fluorescence lifetime of the CDs changed. Through data fitting, the results in Table 1 show that the fluorescence lifetime of the CDs consists of two components. This may be due to the anisotropy of the CDs molecules. In addition, dynamic quenching occurs after the addition of  $\text{Hg}^{2+}$ , and the fluorescence lifetime components change from two components to three components, with the appearance of a short-lived component (approximately 0.58 ns). This further indicates the occurrence of dynamic quenching.

In order to explore the dynamics process of CDs more accurately, we performed transient absorption spectroscopy (Fig. 8). The left two figures show the three-dimensional

transient absorption spectra of CDs before and after the addition of  $\text{Hg}^{2+}$ , and the right figure shows the transient absorption spectra of CDs at typical moments. The components obtained after global fitting and their lifetimes are listed in the Table 2. From the three-dimensional transient absorption spectra, it can be observed that there is excited-state absorption in the range of 500–700 nm, with two excited-state absorption peaks located at 530 and 680 nm, respectively. Weak stimulated emission processes are observed in the range of 450–500 nm. After the addition of  $\text{Hg}^{2+}$ , the excited-state absorption peaks broaden, which is consistent with the changes in the steady-state absorption spectra of the solution before and after the addition of  $\text{Hg}^{2+}$ . The results obtained from the global fitting show that the lifetimes of the three components before the addition of  $\text{Hg}^{2+}$  are 5.86 ps, 69.96 ps, and 6453.72 ps, respectively (Table 2). Among them, the 5.86 ps component corresponds to the process of optical phonon scattering [23–25], the 69.96 ps component corresponds to the process of acoustic phonon scattering [23, 24], and the 6453.72 ps component corresponds to the transition of electrons to the ground state, which can be regarded as the process of radiative transition. After the addition of  $\text{Hg}^{2+}$ , there is photo-induced electron transfer, resulting in a decrease in the lifetimes of the three components [26]. The lifetime of the process of optical phonon scattering decreases from 5.86 ps to 1.08 ps, the lifetime of the process of acoustic phonon scattering decreases from 69.96 ps to 13.26 ps, and the lifetime of the radiative transition process

**Fig. 9** Schematic diagram of energy levels of CDs before and after adding  $\text{Hg}^{2+}$

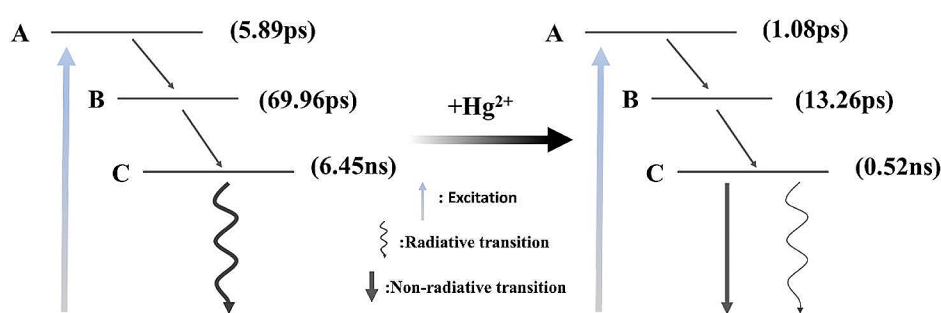


**Table 3** Results of the determination of  $\text{Hg}^{2+}$  in real samples using CDs fluorescent probe ( $n=3$ )

Sample	Added ( $\mu\text{M}$ )	Detected ( $\mu\text{M}$ )	Recovery (%)	RSD (%)
Tap Water	0.2	0.199	99.4	0.177
	0.4	0.405	101.1	1.183
	0.6	0.584	97.3	2.376
Lake Water	0.2	0.203	101.4	0.846
	0.4	0.394	98.6	3.535
	0.6	0.59	98.3	1.478

decreases from 6453.72 ps to 522.3 ps. The result of the radiative transition lifetime is consistent with the measurement result obtained by time-correlated single-photon counting, which verifies the accuracy of the experimental results.

Finally, we obtained the energy level diagram of CDs (Fig. 9). Under the excitation of 407 nm light, the CDs enter the A state, corresponding to the process of optical phonon scattering, with a lifetime of 5.86 ps, and then decay to the B state. B is more like a vibrational relaxed S1 state and the B state corresponds to the process of acoustic phonon scattering, with a lifetime of 69.96 ps, and then decay to the C state, the C state corresponds to the process of electronic transition to the ground state, with a lifetime of 6.45 ns, which also corresponds to the average fluorescence lifetime of the CDs. After the addition of  $\text{Hg}^{2+}$ , the energy levels of the CDs widen due to the complexation between the  $\text{Hg}^{2+}$  and the CDs. Due to the simultaneous occurrence of photo-induced electron transfer, the lifetimes of the A and B states decrease, and non-radiative transition processes of the CDs increase, suppressing the radiative transition process, resulting in fluorescence quenching.

### Detections of $\text{Hg}^{2+}$ in Real Samples

To evaluate the feasibility of detecting  $\text{Hg}^{2+}$  in actual water environments using CDs, we selected laboratory tap water and campus lake water as samples, and filtered and used them as solvents. The recovery rates were measured using the standard addition method, and the results are

shown in Table 3. Within the linear range, the recovery rates for  $\text{Hg}^{2+}$  ranged from 97.3 to 101.4%, with a relative standard deviation (RSD) of less than 3.6%. The experimental results above indicate that this method can accurately determine the concentration of  $\text{Hg}^{2+}$  in practical applications.

### Conclusion

We synthesized a highly sensitive CDs for the detection of  $\text{Hg}^{2+}$  through hydrothermal method. The detection limit (LOD) is as low as 0.024  $\mu\text{M}$ , and the linear detection range is 0.01–1  $\mu\text{M}$ . We also analyzed the mechanism of  $\text{Hg}^{2+}$  quenching CDs fluorescence and found that it mainly includes static quenching and dynamic quenching. In the process of static quenching,  $\text{Hg}^{2+}$  coordinate with the functional groups on the surface of CDs, forming CDs/ $\text{Hg}^{2+}$  ground-state complexes, which significantly reduce the fluorescence emission of CDs at 470 nm. At the same time, photo-induced electron transfer occurs, leading to the quenching of CDs fluorescence. In the practical water environment experiment, the recovery rates reached 97.3–101.4%, indicating the feasibility of this method in practical applications. In summary, this method has the characteristics of simplicity, high sensitivity, and selectivity, making it potential in environmental water quality monitoring. Furthermore, we have gained a clear understanding of the mechanism of CDs fluorescence quenching, which is beneficial to the rational design of CDs-based fluorescence probes.

**Supplementary Information** The online version contains supplementary material available at <https://doi.org/10.1007/s10895-024-03594-z>.

**Author Contributions** Dong Yang: Conceptualization, Methodology, Writing - original draft. Caoqun Ma: Project administration, Funding acquisition, Writing - review & editing. Guoqing Chen: Visualization, Writing - review & editing. Lei Li: Supervision. Anqi Hu: Visualization, Writing - review & editing. Anlan Huang: Visualization, Writing - review & editing. Yan Zhou: Writing - review & editing. Zicheng Cai: Writing - review & editing. Taiqun Yang: Validation, Writing - review & editing. Hui Gao: Data curation. Jiao Gu: Resources. Chun Zhu: Investigation. Yamin Wu: Data curation. All authors read and approved the final manuscript.

**Funding** This work was supported by the Postgraduate Research & Practice Innovation Program of Jiangsu Province [SJCX22\_1102] and the National Natural Science Foundation of China [62105127] & [62375112] & [22004050].

**Data Availability** No datasets were generated or analysed during the current study.

## Declarations

**Competing Interests** The authors declare no competing interests.

**Ethical Approval** Not applicable.

**Consent to Participate** Not applicable.

**Consent to Publish** Not applicable.

## References

- Han Y, Bian Y, Wang G (2023) A novel nitrogen-doped carbon dots as on-off-on fluorescent sensor for ultrasensitive and visual quantitative detection of mercuric (ii) and glutathione. *J Environ Chem Eng* 11(5):110750. <https://doi.org/10.1016/j.jece.2023.110750>
- Fallah S, Baharfard R, Samadi-Maybodi A (2023) Simple and green approach for photoluminescent carbon dots prepared from faba bean seeds as a luminescent probe for determination of Hg<sup>+</sup> ions and cell imaging. *Luminescence* 38(11):1929–1937. <https://doi.org/10.1002/bio.4581>
- Pajewska-Szmyt M, Buszewski B, Gadzała-Kopciuch R (2020) Carbon dots as rapid assays for detection of mercury(ii) ions based on turn-off mode and breast milk. *Spectrochim Acta Part A Mol Biomol Spectrosc* 236:118320. <https://doi.org/10.1016/j.saa.2020.118320>
- Li P, Feng XB, Qiu GL, Shang LH, Li ZG (2009) Mercury pollution in Asia: a review of the contaminated sites. *J Hazard Mater* 168(2):591–601. <https://doi.org/10.1016/j.jhazmat.2009.03.031>
- Liu L, Lin H (2014) Paper-based colorimetric array test strip for selective and semiquantitative multi-ion analysis: simultaneous detection of Hg<sup>2+</sup>, Ag<sup>+</sup> and Cu<sup>2+</sup>. *Anal Chem* 86(17):8829–8834. <https://doi.org/10.1021/ac5021886>
- El Shekheby HA, Mangood AH, Hamza SM, Al Kady AS, Ebeid EZM (2014) A highly efficient and selective turn-on fluorescent sensor for Hg<sup>2+</sup>, Ag<sup>+</sup> and Ag nanoparticles based on a coumarin dithioate derivative. *Luminescence* 29(2):158–167. <https://doi.org/10.1002/bio.2521>
- Wu Y, Ren Y, Guo J, Liu Z, Liu L, Yan F (2020) Imidazolium-type ionic liquid-based carbon quantum dot doped gels for information encryption. *Nanoscale* 12(4):2965–2972. <https://doi.org/10.1039/d0nr06358d>
- Iqbal A, Iqbal K, Xu L, Li B, Gong D, Liu X, Guo Y, Liu W, Qin W, Guo H (2018) Heterogeneous synthesis of nitrogen-doped carbon dots prepared via anhydrous citric acid and melamine for selective and sensitive turn on-off-on detection of hg (ii), glutathione and its cellular imaging. *Sens Actuators B* 255:1130–1138. <https://doi.org/10.1016/j.snb.2017.08.130>
- Rong M, Feng Y, Wang Y, Chen X (2017) One-pot solid phase pyrolysis synthesis of nitrogen-doped carbon dots for Fe<sup>3+</sup> sensing and bioimaging. *Sens Actuators B* 245:868–874. <https://doi.org/10.1016/j.snb.2017.02.014>
- Nannuri SH, Singh S, Chidangil S, George SD (2022) Fluorescence-based detection of mercury ions using carbon dots: role of synthesis route. *Mater Technol (New York N Y)* 37(14):2893–2906. <https://doi.org/10.1080/10667857.2022.2085441>
- Li L, Jiao X, Zhang Y, Cheng C, Huang K, Xu L (2018) Green synthesis of fluorescent carbon dots from Hongcaitai for selective detection of hypochlorite and mercuric ions and cell imaging. *Sens Actuators B* 263:426–435. <https://doi.org/10.1016/j.snb.2018.02.141>
- Cheng S, Wang C, Zhang H, Zou H, Zuo D (2022) Study on the ultraviolet absorbing properties of cotton fabric finished with boron and nitrogen co-doped carbon dots. *J Coat Technol Res* 19(4):1077–1086. <https://doi.org/10.1007/s11998-021-00586-7>
- Rimal V, Singh BK, Mahapatra SS (2023) Phosphoric acid functionalized carbon dots for supercapacitor applications. *Fullerenes Nanotubes and Carbon Nanostructures* 31(11):1096–1103. <https://doi.org/10.1080/1536383X.2023.2241189>
- Sun X, Zhao J, Wang X, Pan W, Yu G, Wang J (2020) The phosphorescence property of carbon dots presenting as powder, embedded in filter paper and dispersed in solid solution. *J Lumin* 218:116851. <https://doi.org/10.1016/j.jlumin.2019.116851>
- Jiang YJ, Lin M, Yang T, Li RS, Huang CZ, Wang J, Li YF (2019) Nitrogen and phosphorus doped polymer carbon dots as a sensitive cellular mapping probe of Nitrite. *J Mater Chem B* 7(12):2074–2080. <https://doi.org/10.1039/c8tb02998a>
- Goswami J, Rohman SS, Guha AK, Basyach P, Sonowal K, Borah SP, Saikia L, Hazarika P (2022) Phosphoric acid assisted synthesis of fluorescent carbon dots from waste biomass for detection of Cr(Vi) in aqueous media. *Mater Chem Phys* 286:126133. <https://doi.org/10.1016/j.matchemphys.2022.126133>
- Pan Y, Wei Z, Ma M, Zhang X, Chi Z, He Y, Wang X, Ran X, Guo L (2022) Broadened optical absorption, enhanced photoelectric conversion and ultrafast carrier dynamics of N, P co-doped carbon dots. *Nanoscale* 14(15):5794–5803. <https://doi.org/10.1039/d2nr00211f>
- Zhao Y, Yu L, Deng Y, Peng K, Huang S (2023) Highly stable n-doped carbon dots as the sensitive probe for the detection of Fe<sup>3+</sup>. *Curr Appl Phys* 50:168–175. <https://doi.org/10.1016/j.cap.2023.04.009>
- Sun X, Zhang J, Wang X, Zhao J, Pan W, Yu G, Qu Y, Wang J (2020) Colorimetric and fluorimetric dual mode detection of Fe<sup>2+</sup> in aqueous solution based on a carbon dots/phenanthroline system. *Arab J Chem* 13(4):5075–5083. <https://doi.org/10.1016/j.arabjc.2020.02.007>
- Luo T, Bu L, Peng S, Zhang Y, Zhou Z, Li G, Huang J (2019) One-step microwave-assisted preparation of oxygen-rich multifunctional carbon quantum dots and their application for Cu<sup>2+</sup>-curcumin detection. *Talanta* 205:120117. <https://doi.org/10.1016/j.talanta.2019.120117>
- Liu C, Yang M, Hu J, Bao L, Tang B, Wei X, Zhao J, Jin Z, Luo Q, Pang D (2021) Quantitatively switchable pH-sensitive photoluminescence of carbon nanodots. *J Phys Chem Lett* 12(11):2727–2735. <https://doi.org/10.1021/acs.jpcclett.1c00287>
- Li H, Han S, Lyu B, Hong T, Zhi S, Xu L, Xue F, Sai L, Yang J, Wang X, He B (2021) Tunable light emission from carbon dots by controlling surface defects. *Chin Chem Lett* 32(9):2887–2892. <https://doi.org/10.1016/j.ccl.2021.03.051>
- Wen X, Yu P, Toh YR, Hao X, Tang J (2013) Intrinsic and extrinsic fluorescence in carbon nanodots: ultrafast time-resolved fluorescence and carrier dynamics. *Adv Opt Mater* 1(2):173–178. <https://doi.org/10.1002/adom.201200046>
- Wang L, Zhu SJ, Wang HY, Wang YF, Hao YW, Zhang JH, Chen QD, Zhang YL, Han W, Yang B, Sun HB (2013) Unraveling bright molecule-like state and dark intrinsic state in green-fluorescence graphene quantum dots via ultrafast spectroscopy. *Adv Opt Mater* 1(3):264–271. <https://doi.org/10.1002/adom.201200020>



25. Huo Z, Chen G, Geng Y, Cong L, Pan L, Xu W, Xu S (2020) A two-photon fluorescence, carbonized polymer dot (CPD)-based, wide range pH nanosensor: a view from the surface state. *Nanoscale* 12(16):9094–9103. <https://doi.org/10.1039/d0nr01543a>
26. Liu C, Tang B, Zhang S, Zhou M, Yang M, Liu Y, Zhang Z, Zhang B, Pang D (2018) Photoinduced electron transfer mediated by coordination between carboxyl on carbon nanodots and  $\text{Cu}^{2+}$  quenching photoluminescence. *J Phys Chem C* 122(6):3662–3668. <https://doi.org/10.1021/acs.jpcc.7b12681>

**Publisher's Note** Springer Nature remains neutral with regard to jurisdictional claims in published maps and institutional affiliations.

Springer Nature or its licensor (e.g. a society or other partner) holds exclusive rights to this article under a publishing agreement with the author(s) or other rightsholder(s); author self-archiving of the accepted manuscript version of this article is solely governed by the terms of such publishing agreement and applicable law.